2008 IEEE International Conference on
Robotics and Automation
Pasadena, CA, USA, May 19-23, 2008

Deployment algorithms for a power-constrained mobile sensor network

Andrew Kwok and Sonia Martínez

Abstract— **This paper presents coverage algorithms for mobile sensor networks in which agents have limited power to move. Rather than making use of a constrained optimization technique, our approach accounts for power constraints by assigning non-homogeneously time-varying regions to each robot. This leads to a novel partition of the environment into limited-range, generalized Voronoi regions. The motion control algorithms are then designed to ascend the gradient of several types of Locational Optimization functions. In particular, the objective functions reflect the global energy available to the group and different coverage criteria. As we discuss in the paper, this has an effect on limiting each agent's velocity to save energy and balance its expenditure across the network.**

I. Introduction

Mobile and static sensor networks hold the promise to impact a large number of applications for exploration, environmental monitoring, safety and recovery operations. It is envisioned that next network generations will make use of small low power mobile devices that operate in a distributed manner [1]. Due to their modest sizes and weights, these systems will have limited resources to divide between communication, computation and motion sub capabilities. Power management becomes a crucial issue for these systems.

One key area of interest regarding mobile sensor networks is deployment to maximize coverage [2], [3], [4], [5], [6]. The ability to dynamically adjust to changes such as agent failure or target acquisition give mobile networks an advantage over static ones. Unfortunately, a drawback to mobile networks is that of power consumption.

Power-aware algorithms have been the subject of extensive research in static sensor networks and mobile middleware, see [7], [8]. To the best of our knowledge, however, limited work on power constraints and deployment has been done in the multi-vehicle sensor network field. The work of [9] and [10] utilize ordinary Voronoi diagrams and a discrete algorithm to show convergence through simulations. Energy considerations enter in their work as total distance traveled until convergence. Another related result from [11], [12] considers a network of agents performing scan lines over a region of interest with energy and time constraints in mind. More involved vehicle energy dynamics are considered in that work, and they address the relevant problem of speed management as well as optimizing the number of agents necessary to provide adequate coverage.

This paper presents a new approach to the distributed deployment problem of mobile sensor networks in which agents have limited energy budgets to move. To account for this, we design algorithms that limit the maximum distance an agent can travel by a dynamically-changing energy radius. This leads to a novel partition of the environment into limited-range, generalized Voronoi regions that produces a more balanced region assignment. Our algorithms seek to maximize objective functions involving: (i) the quantity of coverage as defined by area, and (ii) the quality of coverage as defined by standard Locational Optimization theory [13].

The new partition becomes very useful in order to obtain gradient algorithms that guarantee local maximization of the objective functions. To do so, we consider a kinematic energy expenditure model for each agent. The maximization of the objective functions will then require that agents tune their speed as prescribed by the gradient information. The analysis provided here extends and merges previous work in [14], where coverage algorithms for agents with homogeneous, static sensor ranges is studied, and in [15], where energy partitions for coverage are initially explored disregarding energy constraints on mobility.

We include simulations of each algorithm that show that the corresponding objective functions are maximized. In particular we observe that the basic area-maximizing algorithm may lead to situations where coverage remains constant and yet agents expend energy. To avoid this, we modify our algorithm in two ways: (i) we limit further how fast agents can move but still maximizing the area covered, and (ii) we redesign the algorithms so that a mixed area-centroidal objective coverage function is maximized.

The paper is organized as follows. In Section II we define the problem and present the objective functions that we would like to maximize. In Section III, we present the partition necessary to implement the maximization of the functions in a distributed way with energy constraints. We analyze the objective functions in Section IV, and present their gradient directions. Section V introduces a common gradient ascent algorithm with guaranteed performance to apply to each case. In addition, we address some issues that may arise with such flows. We present simulation results in Section VI and discuss the performance of the algorithms. Finally we point out lines for future research in Section VII.

II. Notation and Problem Definition

Let Q be a convex polytope in $\mathbb{R}^N$ including its interior, and let $\|\cdot\|$ denote the Euclidean norm. We will use $\mathbb{R}_{\geq 0}$ to denote the set of positive real numbers. A map $\phi : Q \to \mathbb{R}_{\geq 0}$, or a *distribution density function*, will represent a measure of a priori known information that some event takes place over Q. Equivalently, we consider Q to be the bounded support of the function ϕ. We denote the interior of a set, $S \subset \mathbb{R}^N$, as $\mathrm{Int}\,(S)$. We will also denote the complement of a set, S, as

A. Kwok is at the department of Mechanical and Aerospace Engineering, Univ. of California, San Diego, 9500 Gilman Dr, La Jolla CA, 92093 ankwok@ucsd.edu

S. Martínez is at the department of Mechanical and Aerospace Engineering, Univ. of California, San Diego, 9500 Gilman Dr, La Jolla CA, 92093 soniamd@ucsd.edu

978-1-4244-1647-9/08/$25.00 ©2008 IEEE.

S^C and its boundary as ∂S. The cardinality of S is denoted as $|S|$. A partition of a region Q is a collection of regions, $\mathcal{A} = (A_1, \ldots, A_n)$, such that: (i), $\mathrm{Int}\,(A_i) \cap \mathrm{Int}\,(A_j) = \emptyset$ for all $i \neq j$ and (ii), $\bigcup_{i=1}^n A_i = Q$.

Let $P = (p_1, \ldots, p_n) \in Q^n$ be the *location of n sensors*, each moving in Q. We interchangeably refer to the elements of the network as sensors, agents, vehicles, or robots. The sensors have initially an associated energy content $(E_1(0), \ldots, E_n(0))$, $0 \leq E_i(0) \leq E_{\max}$, for all $i \in \{1, \ldots, n\}$. Generally, as agents move, their energy reserve will change. We propose the following agent dynamics:

$$\begin{cases} \dot{p}_i = u_i\,, \\ \dot{E}_i = -g_i(\|\dot{p}_i\|)\,, \end{cases} \tag{1}$$

where $\dot{p}_i$ denotes the velocity of agent i such that $\dot{p}_i \in [0, v_{\max}]$, u_i is the control input, and $g_i \colon [0, v_{\max}] \to \mathbb{R}_{\geq 0}$ is any increasing function such that $g(v) = 0$ only at $v = 0$. Intuitively, $g(v)$ captures the fact that energy expenditure increases as velocity increases.

We now formulate the notion of *guaranteed travel range*, the set of points that an agent can reach if it travels in a straight line at any fixed velocity $v_i \in (0, v_{\max}]$ before running out of energy. Without loss of generality, assume $p_i(t_0) = 0$ and $E_i(t_0) > 0$. We wish to find

$$R = \min_{v_i \in (0, v_{\max}]} \|p_i(T)\|\,, \tag{2}$$

where $T > 0$ satisfies $E_i(T) = 0$. From (1), for fixed v_i, we have that $E_i(t) - E_i(t_0) = -g(\|v_i\|)(t - t_0)$, and so

$$T = \frac{E_i(t_0)}{g(\|v_i\|)} + t_0\,. \tag{3}$$

Integrating $\dot{p}_i$ from (1), $p_i(t) = v_i(t - t_0)$. From (2) and (3),

$$R = \min_{v_i \in (0, v_{\max}]} \left\| \frac{E_i(t_0) v_i}{g(\|v_i\|)} \right\|. \tag{4}$$

Note that if $g(\|v_i\|)$ is a polynomial satisfying $g(0) = 0$, then (4) is well-defined. In addition, by definition for any other velocity profile $v_i(t)$ along a straight line path, the resulting travel range $\tilde{R} \geq R$.

For simplicity, we propose the following energy dynamics:

$$\dot{E}_i = -\|\dot{p}_i\|^2 = -\|u_i\|^2\,. \tag{5}$$

Without loss of generality, we can let $v_{\max} = 1$, and from (4), the guaranteed travel range is $R = E_i(t_0)$.

We wish to deploy the robots to maximize a performance metric that quantifies coverage and employs the guaranteed travel ranges for agents. In the most general sense, and motivated by a Locational Optimization approach [13], we seek to maximize a general objective function

$$\mathcal{H}(P, W) = \int_Q \max_i f_i(d_{w_i}(q, p_i))\phi(q)dq\,, \tag{6}$$

where $f_i \colon \mathbb{R} \to \mathbb{R}$ is a non-increasing function, and $d_{w_i} \colon \mathbb{R}^N \times \mathbb{R}^N \to \mathbb{R}$ is some metric function weighted by a scalar $w_i \in \mathbb{R}$, for all $i \in \{1, \ldots, n\}$. These scalars will be associated with the travel ranges for each agent. Depending on the interpretation of coverage $\mathcal{H}$ can be further specialized as we see in the following.

A. Energy-limited coverage

If we interpret coverage to be the set of all reachable points in Q, then under the previous assumptions, the range of an agent $i \in \{1, \ldots, n\}$ is equal to the amount of energy E_i that it has. Let $B_i = B(p_i, E_i)$ be a closed ball centered at p_i with radius E_i and similarly let $S_i = B_i \setminus \mathrm{Int}\,(B_i)$ be a sphere centered at p_i with radius E_i. We will let $\mathcal{R} = Q \cap \bigcup_{i=1}^n B_i$ denote the set of all covered points by the group of agents. We now introduce various objective functions with this new constraint in mind.

Area Coverage: The simplest problem to solve given the energy-limited constraint is to maximize area covered. Therefore, we can set $f_i(x) = 1_{[0, E_i]}(x)$ and $d_{w_i}(q, p_i) = \|q - p_i\|$. Under these assumptions, the general objective function (6) becomes

$$\mathcal{H}_a(P, E) = \int_Q \max_i 1_{[0, E_i]}(\|q - p_i\|)\phi(q)dq = \int_{\mathcal{R}} \phi(q)dq\,. \tag{7}$$

Centroidal Coverage: We can combine the energy-limited range with a typical objective function from Locational Optimization to obtain

$$\mathcal{H}_c(P, E) = \int_{\mathcal{R}} \max_i \{-d_{E_i}(q, p_i)\}\phi(q)dq\,. \tag{8}$$

This has the interpretation of minimizing the mean distance from a point q to an agent at p_i.

Mixed Coverage: We can combine (7) and (8) to strike a balance between quantity of coverage and quality of coverage. We introduce two weights, κ_a, κ_c, to emphasize one over the other. The mixed coverage objective function is

$$\mathcal{H}_m(P, E) = \kappa_a \mathcal{H}_a(P, E) + \kappa_c \mathcal{H}_c(P, E)\,. \tag{9}$$

III. Limited-range, generalized Voronoi regions

In order to come up with local deployment rules for each agent, it is convenient to assign different regions of the space to them. Similarly as in [14], [15], the regions of dominance should reflect each agent's ability to cover an area. In this section we introduce novel partitions of $\mathcal{R}$, $\mathcal{D}^e = (D_1^e, \ldots, D_n^e)$ and $\mathcal{D}^M = (D_1^M, \ldots, D_n^M)$, based on energy motion constraints.

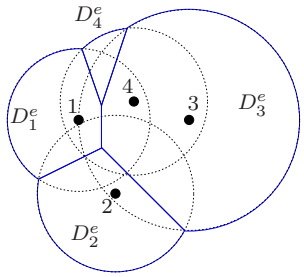

Fig. 1. Proposed partition of $\mathcal{R}$. The individual spheres are shown in dotted lines, along with the boundaries of D_i^e in solid lines.

Let us consider a configuration like the one shown in Figure 1 where $|S_i \cap S_j| > 1$ for all $i \neq j$, $i, j \in \{1, \ldots, n\}$. A possibility is to define D_i^e as the region given by the intersection of B_i with halfplanes, $H(p_i, p_j)$, $\forall\, i \neq j$. The halfplanes $H(p_i, p_j)$ contain p_i and have as

a boundary the line passing through the points in $S_i \cap S_j$. Using a halfplane that contains all such points provides a computationally convenient method of assigning regions of dominance. This intuitive construction can be extended to cases where $|S_i \cap S_j| \in \{1, 0\}$ through the observation provided in the following lemma.

Lemma 1: The intersection of spheres S_i generated by n agents with positions p_i and energies E_i for all $i \in \{1, \ldots, n\}$ induces a natural partition of the space which is the power-weighted Voronoi diagram, $\mathcal{V}^e = (V_1^e, \ldots, V_n^e)$,

$$V_i^e = \{q \in \mathbb{R}^N \mid \|q - p_i\|^2 - E_i^2 \leq \|q - p_j\|^2 - E_j^2\}, \quad (10)$$

for all $i \in \{1, \ldots, n\}$.

•

Boundaries between neighboring points are straight lines in two dimensions, or (hyper-) planes in higher dimensions. Each of these planes divide $\mathbb{R}^N$ into two convex regions. By construction, this indeed creates a partition of $\mathbb{R}^N$. Furthermore, since the intersection of convex regions is also convex, the regions generated by the power-weighted Voronoi partition are convex.

Regarding generalized Voronoi regions, we adopt the following nomenclature. When two Voronoi regions V_i^e and V_j^e are adjacent (i.e., they share an edge), p_i is called a *Voronoi neighbor* of p_j. The set of indices of the Voronoi neighbors of p_i is denoted by $\mathcal{N}_i^e$. Clearly, $j \in \mathcal{N}_i^e$ if and only if $i \in \mathcal{N}_j^e$. We define the (i, j) face as $\Delta_{ij}^e = V_i^e \cap V_j^e$. Note also that a definition for $\mathcal{N}_j^e$ may be obtained from the dual of the power weighted Voronoi region, the power weighted Delaunay graph, $\mathcal{G}_D^e$. The graph $(P, E) \to \mathcal{G}_D^e = (P, \mathcal{E}_D^e(P, E))$ is a type of proximity graph (see [14]) consisting of the vertices P and the edges $\mathcal{E}_D^e(P, E)$ such that

$$\mathcal{E}_D^e(P, E) = \{(p_i, p_j) \in P \times P \setminus \mathrm{diag}(P \times P) \mid V_i^e \cap V_j^e \neq \emptyset\}.$$

In this way, we can define

$$\mathcal{N}_i^e = \{p_j \in P \mid (p_i, p_j) \in \mathcal{E}_D^e(P, E)\}. \quad (11)$$

A. Multiplicatively-weighted Voronoi diagram

Recall from Section II that if $v_i = v_j = v_{\max}$, then two agents must spend all of their energy to reach a point at the intersection of the energy spheres $S_i \cap S_j$. However, both agents do not spend a proportionately equal amount of energy to reach points along the interior of the boundary segments $\Delta_{ij}^e \cap B_i$. We can formulate a new partition, the *multiplicatively-weighted Voronoi partition*, $\mathcal{V}^M = \{V_1^M, \ldots, V_n^M\}$ such that

$$V_i^M = \left\{ q \in \mathbb{R}^N \mid \frac{1}{E_i^2}\|q - p_i\|^2 \leq \frac{1}{E_j^2}\|q - p_j\|^2 \right\}. \quad (12)$$

Thus, given $v_i = v_j = v_{\max}$, agents spend proportionately equal amounts of energy to reach boundary points, $\Delta_{ij}^M = V_i^M \cap V_j^M$. According to [13], for this type of partition generator points lie in their regions, which may not be convex and may be disconnected. The boundaries of these regions are composed of circular arcs. As in the power-weighted case (10), the multiplicatively-weighted Voronoi diagram induces its own limited-range Delaunay graph, $\mathcal{G}_{LD}^M$, with corresponding edges $\mathcal{E}_{LD}^M(P, E)$ and neighbors $\mathcal{N}_i^M$.

Figure 2 compares the power-weighted Voronoi partition with the multiplicatively-weighted one. Notice that the regions of $\mathcal{V}^e$ are convex whereas the regions of $\mathcal{V}^M$ are not.

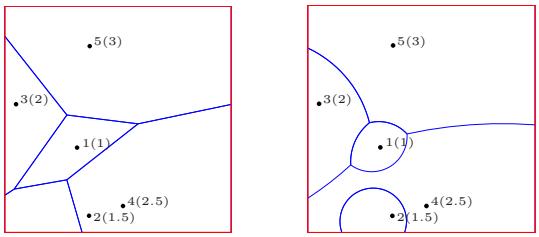

Fig. 2. Comparison of the power-weighted (left) and multiplicatively-weighted (right) Voronoi diagrams. Energy contents are shown in parentheses. Observe that agent 2 is outside its region in the power-weighted case.

B. Limited-range partitions

Thus far, we have proposed two possible partitions of the entire space $\mathbb{R}^N$, (10) and (12). We now incorporate these two partitions with the limited range concept from Section II.

In order to partition $\mathcal{R} = \bigcup_{i=1}^n B_i$, we propose that each element of $\mathcal{D}^e = (D_1^e, \ldots, D_n^e)$ be defined as $D_i^e = B_i \cap V_i^e$, $i \in \{1, \ldots, n\}$. Agent regions of dominance, D_i^e, will have boundaries that consist of Voronoi face segments, $\Delta_{ij}^e \cap B_i$, and energy radius arcs. We will refer to the union of all those arcs as $\mathrm{Arcs}(D_i^e)$, which gives $\partial D_i^e = \bigcup_{j \in \mathcal{N}_i^e} (\Delta_{ij}^e \cap B_i) \cup \mathrm{Arcs}(D_i^e)$. This proposed partition will also have a dual graph, the energy limited Delaunay graph $\mathcal{G}_{LD}^e = (P, \mathcal{E}_{LD}^e(P, E)$. The edge set is defined as

$$\mathcal{E}_{LD}^e(P, E) = \{(p_i, p_j) \in P \times P \setminus \mathrm{diag}(P \times P) \mid V_i^e \cap V_j^e \neq \emptyset, \|p_i - p_j\| \leq E_i + E_j\}.$$

The set of neighbors is defined similar to (11). In addition, we will define the quantities M_i^e and C_i^e as the *mass* and *centroid* of the region D_i^e,

$$M_i^e = \int_{D_i^e} \phi(q) dq, \qquad C_i^e = \frac{1}{M_i^e} \int_{D_i^e} q\phi(q) dq. \quad (13)$$

A similar treatment for the multiplicatively weighted Voronoi diagram yields $\mathcal{D}^M = (D_1^M, \ldots, D_n^M)$ where $D_i^M = B_i \cap V_i^M$. Boundaries of D_i^M will be composed of Voronoi face arcs $\Delta_{ij}^M \cap B_i$ and energy radius arcs $\mathrm{Arcs}(D_i^M)$. The proposed partition $\mathcal{D}^M$ will also have its own dual graph $\mathcal{G}_{LD}^M$ with edge set $\mathcal{E}_{LD}^M$. Analogous to (13), we define the mass and centroid of each region D_i^M as M_i^M and C_i^M, respectively.

It can be verified that $\mathcal{D}^e$ and $\mathcal{D}^M$ are in fact partitions, and we state the following theorem for clarity.

Theorem 2: Let $\mathcal{D}^e = \{D_1^e, \ldots, D_n^e\}$ be a collection of sets with $D_i^e = B_i \cap V_i^e$. Let $\mathcal{D}^M = \{D_1^M, \ldots, D_n^M\}$ with $D_i^e = B_i \cap V_i^e$. Then, $\mathcal{D}^e$ and $\mathcal{D}^M$ are partitions of $\bigcup_{i=1}^n B_i$.

The two partitions of $\mathcal{R}$ yield similar results as can be seen in Figure 3. Generally speaking, the power-weighted partition

$\mathcal{D}^e$ is a good approximation to the multiplicatively-weighted partition $\mathcal{D}^M$ if the agents are spaced far enough apart, or if the energy contents of neighbors are similar. Regions of $\mathcal{D}^e$ are convex and it is computationally simpler to construct regions, which may be a consideration in applications where processing power is limited. The rest of this paper will present results based off of the approximate partition $\mathcal{D}^e$.

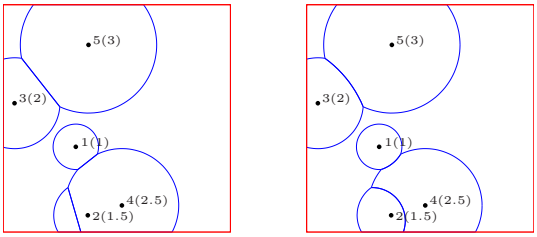

Fig. 3. Comparison of the limited range power-weighted (left) and multiplicatively-weighted (right) partitions, for the same set of points from Figure 2. Energy contents are shown in parentheses.

IV. Objective function gradient characterization

In this section we derive the gradient direction for each of the three objective functions that we have introduced previously. These gradients define the proper direction of flow in order to optimize coverage. Before computing the gradients we would like to note the following result.

Lemma 3: The objective functions derived from (6) are continuously differentiable.

In addition, with a clear definition of the partitioning of $\mathcal{R}$, we now specify the weighted distance metric found in (8) as

$$d^e_{E_i}(q,p_i) = \|q-p_i\|^2 - E_i^2\,, \tag{14}$$

for the partition $\mathcal{D}^e$. We can now rewrite the objective functions: (7) and (8). Specifically, using $\mathcal{D}^e$, we have

$$\mathcal{H}_a(P,E) = \sum_{i=1}^{n}\int_{D_i^e}\phi(q)dq\,, \tag{15}$$

$$\mathcal{H}_c(P,E) = \sum_{i=1}^{n}\int_{D_i^e} -\left(\|q-p_i\|^2 - E_i^2\right)\phi(q)dq\,. \tag{16}$$

We now state the gradient expressions for these functions.

Proposition 4: Consider the objective functions $\mathcal{H}_a$, $\mathcal{H}_c$, and $\mathcal{H}_m$ from (15), (16), and (9), respectively using the partition $\mathcal{D}^e$. Let $X = (X_1,\ldots,X_n)$ be a general vector field where

$$X_i = (X_{p_i}, X_{E_i}) : Q\times\mathbb{R}\to\mathbb{R}^N\times\mathbb{R}\,,$$

for all $i\in\{1,\ldots,n\}$. Then, the Lie derivatives of $\mathcal{H}_a$, $\mathcal{H}_c$, and $\mathcal{H}_m$ along the flow X are:

$$\mathcal{L}_X\mathcal{H}_a = \sum_{i=1}^{n}\left(\int_{\text{Arcs}\left(D_i^e\right)}\phi(\gamma_i)[n^t(\gamma_i)]^T d\gamma_i\right)X_{p_i} + \left(\int_{\text{Arcs}\left(D_i^e\right)}\phi(\gamma_i)d\gamma_i\right)X_{E_i}\,, \tag{17}$$

$$\mathcal{L}_X\mathcal{H}_c = \sum_{i=1}^{n}\left(2M_i^e(C_i^e - p_i)^T\right)X_{p_i} + (2E_iM_i^e)X_{E_i} \tag{18}$$

$$\mathcal{L}_X\mathcal{H}_m = \kappa_a\mathcal{L}_X\mathcal{H}_a + \kappa_c\mathcal{L}_X\mathcal{H}_c\,, \tag{19}$$

Remark 5: The gradient expressions can be derived for the multiplicatively-weighted partitions $\mathcal{D}^M$ in an analogous fashion as (17), (18), and (19). They are, however, slightly more complicated. A control law and convergence result can be reached analogous to the results of the following section.

V. Gradient-ascent deployment algorithms

Once we have computed the gradient directions for each objective function, we will apply a gradient-ascent control algorithm for each case. Consider (1) with

$$u_i = k(p_i,E_i)\,\text{sat}\left(\frac{\partial\mathcal{H}}{\partial p_i}\right)\,, \tag{20}$$

where the saturation function is

$$\text{sat}(v) = \begin{cases} v & ,\|v\|\le 1\,,\\ \frac{v}{\|v\|} & ,\|v\|>1\,.\end{cases}$$

Here the control gain $k(p_i,E_i)\ge 0$ serves to modulate the velocity of each agent along its gradient climbing path.

Now we analyze the time evolution of the resulting objective function with this law. We adopt the shorthand notation $k_i = k(p_i,E_i)$. Combining the gradient direction with the time derivatives above, we get the following Lie derivative for an objective function

$$\begin{aligned}\frac{d\mathcal{H}}{dt} &= \sum_{i=1}^{n}\frac{\partial\mathcal{H}}{\partial p_i}\dot{p}_i + \frac{\partial\mathcal{H}}{\partial E_i}\dot{E}_i \\ &= \sum_{i=1}^{n}k_i\frac{\partial\mathcal{H}}{\partial p_i}\cdot\text{sat}\left(\frac{\partial\mathcal{H}}{\partial p_i}\right) - k_i^2\frac{\partial\mathcal{H}}{\partial E_i}\left\|\text{sat}\left(\frac{\partial\mathcal{H}}{\partial p_i}\right)\right\|^2 \\ &= \sum_{i=1}^{n}k_i\,\text{sat}\left(\frac{\partial\mathcal{H}}{\partial p_i}\right)\cdot\left(\frac{\partial\mathcal{H}}{\partial p_i} - k_i\frac{\partial\mathcal{H}}{\partial E_i}\,\text{sat}\left(\frac{\partial\mathcal{H}}{\partial p_i}\right)\right)\,.\end{aligned} \tag{21}$$

Remark 6: Non-smooth dynamics are also possible:

$$\dot{p}_i = k(p_i,E_i)\frac{\frac{\partial\mathcal{H}}{\partial p_i}}{\left\|\frac{\partial\mathcal{H}}{\partial p_i}\right\|}\,,$$
$$\dot{E}_i = -\|\dot{p}_i\|^2 = -k^2(p_i,E_i)\,.$$

Doing so would require the non-smooth analysis techniques found in [16]. We would, however, arrive at the same convergence conclusions found in the next subsections. •

A. Optimal gain selection

We wish that $\frac{d\mathcal{H}}{dt}\ge 0$ since we are maximizing the objective function. We now derive a sufficient condition for k and also present an optimal choice for k.

Lemma 7: Given the model (1), (20), and an objective function $\mathcal{H}$, the latter is maximized if

$$0\le k(p_i,E_i)\le\frac{\text{sat}\left(\frac{\partial\mathcal{H}}{\partial p_i}\right)\cdot\frac{\partial\mathcal{H}}{\partial p_i}}{\left\|\text{sat}\left(\frac{\partial\mathcal{H}}{\partial p_i}\right)\right\|^2\frac{\partial\mathcal{H}}{\partial E_i}}\,, \tag{22}$$

for all $i \in \{1, \ldots, n\}$, and an optimal choice of $k(p_i, E_i)$ is

$$k^*(p_i, E_i) = \frac{1}{2} \frac{\text{sat}\left(\frac{\partial \mathcal{H}}{\partial p_i}\right) \cdot \frac{\partial \mathcal{H}}{\partial p_i}}{\left\|\text{sat}\left(\frac{\partial \mathcal{H}}{\partial p_i}\right)\right\|^2 \frac{\partial \mathcal{H}}{\partial E_i}}. \tag{23}$$

Remark 8: Different energy dynamics can be considered as in [12] where energy dynamics are modeled using a fourth order polynomial in $\dot{p}_i$. More complex dynamics are allowable if they are sufficiently smooth with respect to $\dot{p}_i$.•

Although using (23) provides the quickest rate of convergence, it may not be the best. Consider the situation shown in Figure 4, for the case where the objective function is (7). Agent 4 has a small arc component compared to its entire boundary. However with the area coverage gradient (17), the optimal gain (23) remains constant since $\frac{\partial \mathcal{H}_a}{\partial p_i}, \frac{\partial \mathcal{H}_a}{\partial E_i} \to 0$ at the same rate. For this reason, we would like k_i to be chosen by the following constrained optimization way: maximize the summand of (21) subject to $k_i \leq \frac{\partial \mathcal{H}}{\partial E_i}$. Notice that this quantity is of the form $f(k_i) = k_i(c_1 - k_i c_2)$, a concave parabola. With this constraint, the optimum k_i^* is then

$$k_i^* = \min \left\{ \frac{1}{2} \frac{\text{sat}\left(\frac{\partial \mathcal{H}}{\partial p_i}\right) \cdot \frac{\partial \mathcal{H}}{\partial p_i}}{\left\|\text{sat}\left(\frac{\partial \mathcal{H}}{\partial p_i}\right)\right\|^2 \frac{\partial \mathcal{H}}{\partial E_i}}, \frac{\partial \mathcal{H}}{\partial E_i} \right\}. \tag{24}$$

A simulation in Section VI further discusses this choice.

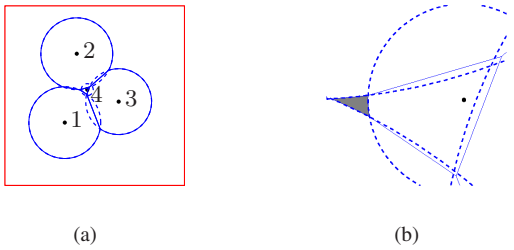

(a) (b)

Fig. 4. Agent number 4 in (a), has a small arc component compared to its total boundary mass. The shaded area in (b) does not belong in the region of any agent. The energy radii, E_i, are shown as dotted lines.

Remark 9: We discuss what information agents would need to know in order to implement a control law as in (20) in a distributed way. In order for vehicle i to correctly construct a region D_i^e, it must receive position and energy information (p_j, E_j) from neighbors such that $(p_i, p_j) \in \mathcal{E}_{LD}^e(P, E)$. A sufficient condition to achieve this is if p_j can transmit to p_i when $\|p_i - p_j\| \leq 2E_m$ for all $j \neq i$. With this communication requirement, the control law described in (20) is spatially distributed over the graph $\mathcal{G}_{LD}^e$; i.e. in order to implement its motion control rule p_i only needs to know information about its neighbors in $\mathcal{G}_{LD}^e$. •

B. Convergence analysis

We now replace the general objective, $\mathcal{H}$, with the functions developed in (7), and (9). The proof of the following theorem relies on the LaSalle invariance principle (see [17]).

Theorem 10 (Critical configurations and convergence): The critical points of a gradient ascent flow characterized by (20) and appropriate choice of k using an objective function $\mathcal{H} \in \{\mathcal{H}_a, \mathcal{H}_c, \mathcal{H}_m\}$ are configurations where each agent either satisfies $\frac{\partial \mathcal{H}}{\partial p_i} = 0$, or has no energy, $E_i = 0$. The statement $\frac{\partial \mathcal{H}}{\partial p_i} = 0$ has the following meanings:

(i) the vehicle cannot further locally increase its coverage area when using $\mathcal{H}_a$,
(ii) vehicle i is located at the centroid of D_i^e when using $\mathcal{H}_c$, and
(iii) the vehicle has reached a balance between maximizing area covered and remaining close to the centroid of D_i^e when using $\mathcal{H}_m$.

Agents approach these critical configurations as $t \to \infty$.

VI. Simulations

In this section, we present simulation results for the three coverage objectives. First, however, we will address the motivation for choosing k_i^* from (24) over (23). In this simulation, $n = 8$ agents were initialized at random initial positions with $E_i = 10$ for $i \in \{1, \ldots, 8\}$. The agents were confined to $Q = [0, 15] \times [0, 15] \subset \mathbb{R}^2$ with $\phi(x, y) = 1 + 10 \exp[-\frac{1}{9}((x-10)^2 + (y-10)^2)]$. The agents maximized the area coverage objective function (7).

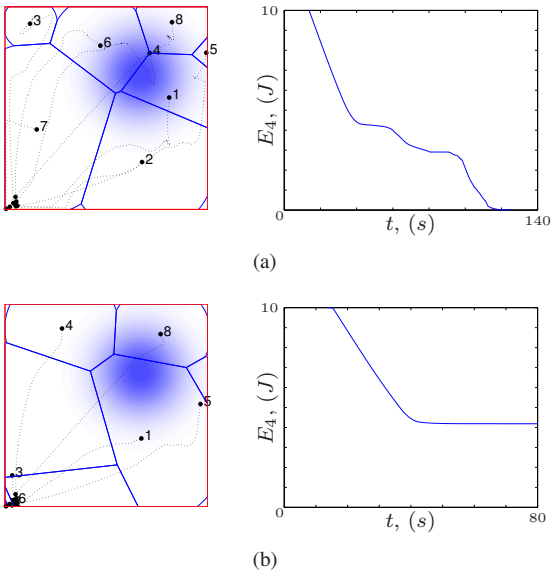

Fig. 5. Comparison between the performance of k_i^* from (23), (a); and from (24), (b). Agent paths and final configurations are shown at left, and the energy level of agent 4 is plotted at right. Shaded regions indicate a high value of ϕ.

The use of k_i^* from (24) demonstrates a couple advantages over (23) in the simulation of Figure 5. In Figure 5(a), agent 4 finishes with almost no energy, while the same agent has significantly more energy in Figure 5(b). In addition, all 8 agents were deployed in Figure 5(a) while only 5 agents left the starting location in Figure 5(b).

We first examine the area coverage case, (7). Here, $n = 12$ agents are confined to $Q = [0, 10] \times [0, 10] \subset \mathbb{R}^2$ with a density function ϕ composed of 4 Gaussian distributions (see Figure 6). The density function used was

$$\phi(q) = 1 + 10\Big[e^{-\frac{\|q-r_1\|^2}{9}} + e^{-\frac{\|q-r_2\|^2}{2}} + e^{-\frac{\|q-r_3\|^2}{2}} + e^{-\|q-r_4\|^2}\Big],$$

where $r_1 = (8, 8)$, $r_2 = (8, 2)$, $r_3 = (8, 4)$ and $r_4 = (3, 7)$. Agents started at random positions in the lower-left corner, with $E_i = 3$ for $i \in \{1, \ldots, 12\}$. The agents followed the gradient ascent control law in (20), and used (24).

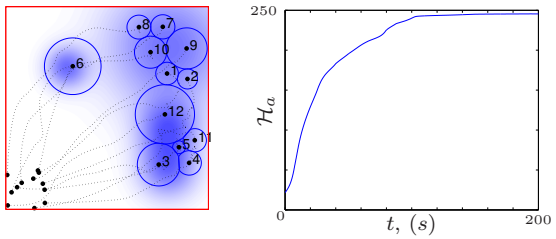

Fig. 6. Area coverage simulation results. The path lines and final configurations are shown at the left; shaded regions indicate a high value of ϕ. The cost function for the entire system, $\mathcal{H}_a$, is plotted on the right. The average energy content at the end of the simulation was 0.79.

The area coverage simulation increased the coverage of Q as time progressed, Figure 6 (right). Because the gradient tends to push agents away from each other, small holes of uncovered area remain, such as the space between agents $1, 2, 3, 4$. Also, the agents had an average energy level of 0.79 at the end of the simulation. We will see in the mixed coverage case that this is improved upon.

The second simulation presents the mixed-coverage case (9) with identical initial conditions. The area and centroidal components carried equal weight, $\kappa_a = \kappa_c = 1$ from (9). Agents performed better in terms of final energy content, with an average of 1.50 at the end of the simulation. Qualitatively, there are fewer coverage holes compared to the previous simulation. The centroidal component of $\mathcal{H}_m$ "forces" agents towards the denser regions of ϕ, overcoming the repulsive area-maximizing component of $\mathcal{H}_m$.

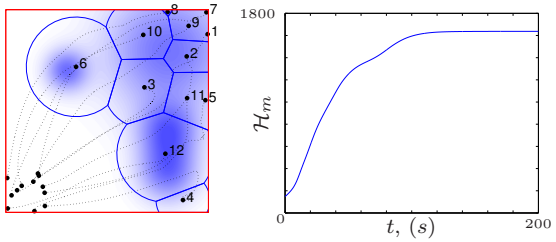

(a)

Fig. 7. Mixed centroid and area coverage simulation results. The path lines and final configurations are shown at left; shaded regions correspond to higher values of ϕ. The global cost function $\mathcal{H}_m$ is plotted at the right. The average energy content at the end of the simulation was 1.50.

VII. Conclusions

We have presented a novel set of spatially distributed coverage control algorithms. We designed three objective functions to demonstrate the flexibility of this method. In addition each of these algorithms place an emphasis on individual energy levels through use of a generalized Voronoi partition. We have shown through simulation that the three cases that we developed perform as intended.

Current work includes developing an implementation of the multiplicatively-weighted Voronoi partition. In addition, incorporating nonholonomic vehicle dynamics into the convergence analysis would provide a more practical scenario. In the future we will implement these ideas in a physical testbed as well. We are currently working on algorithms that help us find a global optima.

VIII. Acknowledgments

This material is based upon work supported by NSF Awards CMS-0643673 and IIS-0712746.

References

[1] D. Estrin, D. Culler, K. Pister, and G. Sukhatme, "Connecting the physical world with pervasive networks," *IEEE Pervasive Computing*, vol. 1, no. 1, pp. 59–69, 2002.

[2] J. Cortés, S. Martínez, T. Karatas, and F. Bullo, "Coverage control for mobile sensing networks," *IEEE Transactions on Robotics and Automation*, vol. 20, no. 2, pp. 243–255, 2004.

[3] A. Howard, M. J. Matarić, and G. S. Sukhatme, "Mobile sensor network deployment using potential fields: A distributed scalable solution to the area coverage problem," in *International Conference on Distributed Autonomous Robotic Systems (DARS02)*, Fukuoka, Japan, June 2002, pp. 299–308.

[4] S. Poduri and G. S. Sukhatme, "Constrained coverage for mobile sensor networks," in *IEEE Int. Conf. on Robotics and Automation*, 2004, pp. 165–172.

[5] C. Belta and V. Kumar, "Abstraction and control for groups of robots," *IEEE Transactions on Robotics*, vol. 20, no. 5, pp. 865–875, 2004.

[6] M. Schwager, J. McLurkin, and D. Rus, "Distributed coverage control with sensory feedback for networked robots," in *Proceedings of Robotics: Science and Systems*, August 2006.

[7] V. Raghunathan, C. Pereira, M. Srivastava, and R. Gupta, "Energy-aware wireless systems with adaptive power-fidelity tradeoffs," *IEEE Trans. Very Large Scale Integration Systems*, vol. 13, no. 2, pp. 211–225, February 2005.

[8] S. Mohapatra, N. Dutt, A. Nicolau, and N. Venkatasubramanian, "DYNAMO: A cross-layer framework for end-to-end QoS and Energy Optimization in Mobile Handheld Devices," *IEEE J. Selected Areas in Communication*, May 2007.

[9] N. Heo and P. K. Varshney, "Energy-efficient deployment of intelligent mobile sensor networks," *IEEE Transactions on Systems, Man and Cybernetics, Part A*, vol. 35, no. 1, pp. 78–92, January 2005.

[10] G. Wang, G. Cao, and T. L. Porta, "Movement-assisted sensor deployment," *IEEE Transactions on Mobile Computing*, pp. 640–652, June 2006.

[11] Y. Mei, Y. Lu, Y. Hu, and C. Lee, "Determining the fleet size of mobile robots with energy constraints," in *IEEE/RSJ Int. Conf. on Intelligent Robots & Systems*, vol. 2, 2004, pp. 1420–1425.

[12] ——, "Deployment of mobile robots with energy and timing constraints," *IEEE Transactions on Robotics*, vol. 22, no. 3, pp. 507–522, June 2006.

[13] A. Okabe, B. Boots, K. Sugihara, and S. N. Chiu, *Spatial Tessellations: Concepts and Applications of Voronoi Diagrams*, 2nd ed., ser. Wiley Series in Probability and Statistics. New York: John Wiley, 2000.

[14] J. Cortés, S. Martínez, and F. Bullo, "Spatially-distributed coverage optimization and control with limited-range interactions," *ESAIM. Control, Optimisation & Calculus of Variations*, vol. 11, pp. 691–719, 2005.

[15] A. Kwok and S. Martínez, "Energy-balancing cooperative strategies for sensor deployment," in *IEEE International Conference on Decision and Control*, New Orleans, USA, December 2007, pp. 6136–6141.

[16] J. Cortés, "Finite-time convergent gradient flows with applications to network consensus," *Automatica*, vol. 42, no. 11, pp. 1993–2000, November 2006.

[17] H. K. Khalil, *Nonlinear Systems*, 3rd ed. Prentice Hall, 2001.